

# Ultrathin Nanogenerators as Self-Powered/Active Skin Sensors for Tracking Eye Ball Motion

Sangmin Lee, Ronan Hinchet, Yean Lee, Ya Yang, Zong-Hong Lin, Gustavo Ardila, Laurent Montès, Mireille Mouis, and Zhong Lin Wang\*

**Ultrathin piezoelectric nanogenerator (NG) with a total thickness of  $\approx 16 \mu\text{m}$  is fabricated as an active or self-powered sensor for monitoring local deformation on a human skin. The NG was based on an anodic aluminum oxide (AAO) as an insulating layer grown on a thin Al foil by anodization, on which a thin film made of aligned ZnO nanowire compacted arrays is grown by solution chemistry. The performance of the NG is characterized with the assistance of the finite element method (FEM) simulation. The extremely thin NG is attached on the surface of an eyelid, and its output voltage/current characterizes the motion of the eye ball underneath. Since there is no external power needed for the operation of the NG, this self-powered or active sensor can be effective in monitoring sleeping behavior, brain activities, and spirit status of a person as well as any biological associated skin deformation.**

## 1. Introduction

Self-powered systems that are operated without external power sources are attracting a vast interest due to the exceedingly increase in the number of personal/portable electronics.<sup>[1]</sup> One of the most important approaches for the self-powered system is to harvest the operation energy from the ambient environment. Some types of energy sources, such as solar, thermal, and mechanical energies, are common in our surroundings and have been utilized for generating electricity.<sup>[2–4]</sup> Mechanical energy is one of the most desirable sources because it can be consistently used with no constrain of time and location. In recent years, piezoelectric nanogenerators (NGs) have been developed as a promising approach for harvesting random mechanical energy due to vibration, mechanical triggering, and

human motion.<sup>[5–10]</sup> The output from the NG is an electric signal that characterizes the applied mechanical agitation, which can be used in two ways. One way is the output electric power as stated above. The other is that it can be used as a sensor signal for detecting magnitude and rate of the mechanical deformation. Since no power is applied in the signal detection, sensors based on NGs are called active or self-powered sensors, and they have been demonstrated for monitoring heart-pulse, tire pressure, cantilever vibration frequency, ambient wind-velocity detection, transportation, and skin deformation.<sup>[11–16]</sup>

The working mechanism of the NG relies on the piezoelectric potential created in piezoelectric nanowires (NWs) when they are dynamically strained by an external force, and the corresponding charge carriers flow through an external load in order to balance the potential. In the NG device, a thin poly(methyl methacrylate) (PMMA) layer coated on the NWs provides an infinite potential barrier between the NWs and the metal electrode for charge accumulation and preventing them from transporting through the ZnO/metal interface.<sup>[17]</sup> The reported NGs typically have thicknesses in a range of 1–3 mm, which normally consumes a large percentage of input mechanical energy when subjects to deformation. It is desirable to fabricate ultrathin NGs in order to enhance either their power conversion efficiency or sensitivity as sensors.

Here, we report an ultrathin NG of total thickness  $\approx 16 \mu\text{m}$  as an active sensor for detecting tiny skin deformation. The NG was fabricated based on an ultrathin Al foil, on which anodic aluminum oxide (AAO) was created to serve as a blocking layer for electron transport between the Al electrode and the grown ZnO nanowire film. The super-flexible NG demonstrated its great potential to work as an active deformation sensor capable of detecting the eye ball movement when it was attached on the surface of the eyelid for monitoring sleep pattern, tiredness and possible brain activity. The super-flexible NG can be applied to the surface of a biological object of any shape due to its high conformability.

## 2. Results and Discussion

Figure 1a shows a schematic diagram of the fabricated super-flexible NG. For an insulating AAO layer, the Al foil with the thickness of  $\approx 18 \mu\text{m}$  (99.5%) was used as an electrode. In order

Dr. S. Lee, Dr. Y. Yang, Dr. Z.-H. Lin, Prof. Z. L. Wang  
School of Materials Science and Engineering  
Georgia Institute of Technology  
Atlanta, GA, 30332-0245, USA

R. Hinchet, Dr. G. Ardila, Dr. L. Montès, Dr. M. Mouis  
IMEP-LAHC, Grenoble INP – Minatoc, 3 rue Parvis,  
Louis Néel, 38016, Grenoble

Y. Lee  
Department of Mechanical Engineering  
Georgia Institute of Technology  
Atlanta, GA, 30332-0245, USA

Prof. Z. L. Wang  
Beijing Institute of Nanoenergy and Nanosystems  
Chinese Academy of Sciences  
Beijing, China  
E-mail: zlwang@gatech.edu



DOI: 10.1002/adfm.201301971

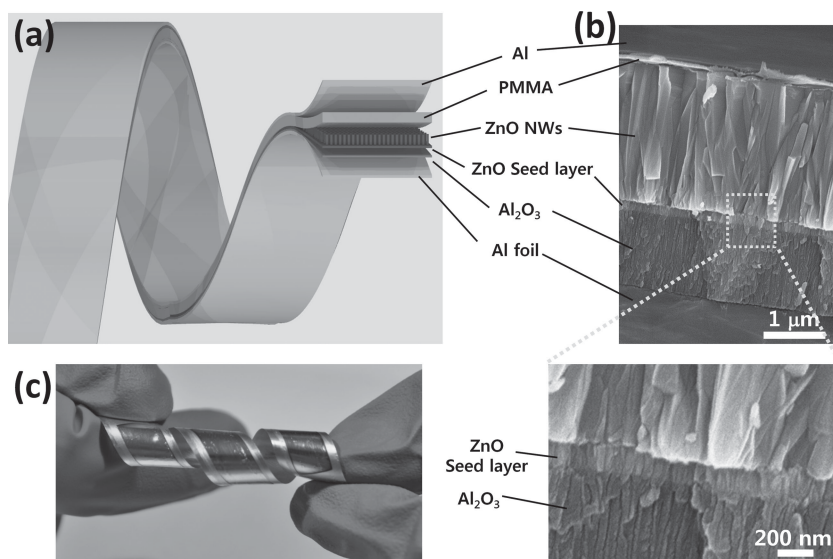


**Figure 1.** Super-flexible piezoelectric nanogenerator (NG). a) Scheme of the super-flexible NG based on an anodic aluminum oxide (AAO) as an insulating layer. The AAO layer was grown on an ultrathin Al foil prior to the growth of ZnO NWs in order to lead to high-sensitivity and durability of the NG as well as high-throughput process due to the covalent bonds by sharing oxygen atoms and the increased surface contact area by the nanopores of the AAO layer between the AAO and the ZnO seed layer. b) SEM and the enlarged SEM images of cross section of the NG. c) Optical image of the twisted super-flexible NG.

to fabricate some NG devices at once without any electrical problems, such as short circuit or electrical leakage, an adhesive tape was applied on the Al foil (see Supporting Information, Figure S1), and then the Al foil was anodized. In the anodization process, AAO layers with nanometer pores were fabricated on both surfaces of the Al foil (Supporting Information, Figure S2). In order to cover up the AAO surface with nanopores for the growth of ZnO NWs, 100-nm thick ZnO seed layer was sputtered on the surface. Then, ZnO NWs were grown on the seed layer by a hydrothermal process. The ZnO NWs were densely grown on the ZnO seed-coated AAO layer (Supporting Information, Figure S3). In this study, the AAO layer was grown on the Al foil as an insulating layer, which created enhanced adhesion between the ZnO seed layer and the AAO due to not only the covalent bond by sharing oxygen atoms but also the increased surface contact area caused by the nanopores of the AAO layer compared to the previous study (Supporting Information, Figure S4).<sup>[16,18]</sup> In addition, since there was little difference in thermal expansion between them during the hydrothermal process, mechanically stable NG device was able to be fabricated. A thin layer of PMMA (MicroChem 950k A2) was spun-coated on the surface of the as-grown ZnO NWs (at a speed of 1000 rpm) to effectively transmit the bending force to all NWs through the PMMA layer. A 50-nm-thick

Al layer was sputtered on the surface of the PMMA layer, serving as the top electrode of the NG. Finally, by removing the adhesive tape and cutting the part previously covered by the tape, multiple NG devices were easily fabricated at once without any electrical problems, such as short circuit or electrical leakage. The cross-section of the fabricated NG was confirmed by field emission scanning electron microscopy (FE-SEM) images, as shown in Figure 1b. Figure 1c shows an optical image of the twisted super-flexible NG with the thickness of about 16  $\mu\text{m}$ .

The thin insulating layer plays a key role in the working mechanism of the NG by creating a high potential barrier between the ZnO NWs and the electrode. This barrier protects the NG from short circuiting, but it remains some electrical effects such as dielectric losses and screening effect that can affect the output performances of the NG. Also, since the NG acts as a charged capacitor, the capacitance of the device and the generated current vary with the thickness of the insulating layer. In order to investigate the effect of the thickness of the AAO layer on the NG, finite element method

(FEM) simulation was carried out using the ZnO NW arrays ( $15 \times 15$ ) for  $\text{Al}_2\text{O}_3$  layer thicknesses of 100, 300, 600, 900, 1200, 1500, and 2000 nm (Figure 2a and Supporting Information, Figure S5). The NG device was composed of PMMA,

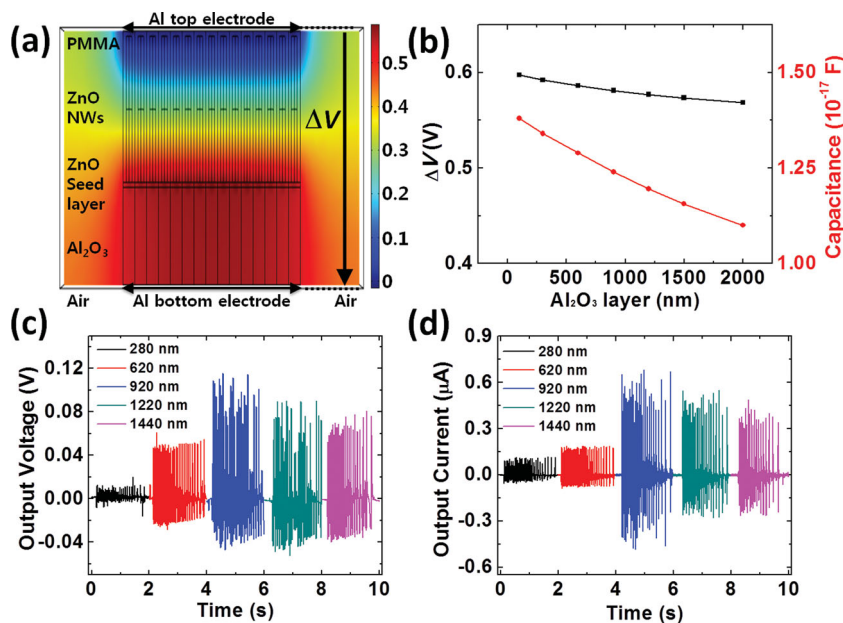


**Figure 2.** Dependence of the NG output performance on the thickness of the insulating AAO layer. a) FEM simulation of electric potential distribution in the entire NG. b) FEM simulated potential difference and the capacitance between the top and the bottom Al electrodes ( $\Delta V$ ) as a function of the thickness of the insulating AAO layer. Experimental results of the c) output voltage and d) current for the NGs with different thicknesses of the insulating AAO layer measured under the same experimental conditions.

ZnO NWs, ZnO seed layer, and  $\text{Al}_2\text{O}_3$ . As shown in Figure 2b, the simulation result shows that the difference of the voltage between the top and the bottom Al electrodes ( $\Delta V$ ) was slightly decreased as the thickness of the  $\text{Al}_2\text{O}_3$  layer increased due to the dielectric loss in the insulator. The capacitance of the  $\text{Al}_2\text{O}_3$  layer is inversely proportional to its thickness, and the capacitance decrease leads to a drop in the total capacitance of the NG device (see Figure 2b).

Before the demonstration of these results, in order to exclude the effect of a change in capacitance under the external force, which could cause output signals related to effects within the measurement system, we prepared the device without ZnO NWs for comparison. The electric signal generated by the device was much smaller than that from the device with ZnO NWs, and the result demonstrated that the signal was indeed from the piezoelectric effect of the ZnO NWs. (Supporting Information, Figure S6) To demonstrate the simulation results, the five NG devices with different AAO layer thicknesses of 280, 620, 920, 1220, and 1440 nm, were prepared by controlling the anodizing time (Supporting Information, Figure S7). To characterize the performance of the NG devices, the NG was tested by a controllable trigger setup, which could periodically bend and unbend under the same condition.<sup>[10]</sup> The NG was set up such that the ZnO NW layer was compressively strained. Firstly, when the thickness of the AAO layer was larger than 920 nm, the output voltage decreased as the thickness increased, showing similar tendency with the simulation results. As the thickness of the AAO layer increased from 920, 1220 to 1440 nm, the output voltage decreased from  $\approx 0.11$  V,  $\approx 0.09$  V, and to  $\approx 0.075$  V, respectively (see Figure 2c). In addition, the output current showed a similar trend because of the role of the output voltage in the current equation  $I = dQ/dt = d(CV)/dt$  and the capacitance decrease of the NG device as the thickness of the AAO layer increased (see Figure 2b,d). However, when we assumed that the AAO layer was a perfect insulator, the simulation result showed that the  $\Delta V$  slightly decreased as the thickness of the AAO layer increased due to the dielectric loss in the insulator. In general, the dielectric losses are affected by the dielectric constant of the material and the geometry of the device. In our case, considering the theoretical relative permittivity of  $\text{Al}_2\text{O}_3$ , the effect of the dielectric losses will be minimal because of the high aspect ratio ( $\approx 625$ ) of the width ( $\approx 1$  cm) to the thickness ( $\approx 16$   $\mu\text{m}$ ) of the NG device. Hence, there may be another reason for the decreased voltage output in our devices as the thickness of the AAO layer increased. Secondly, the NG with the AAO layer thinner than 920 nm showed that the output voltage and the current increased with the thickness of the AAO layer unlike the simulation result, as shown in Figure 2c,d. The reason for the different tendency between experimental and simulation results in this range is possibly due to a current leakage occurred through the AAO layer. The AAO layer is probably not perfect insulator and it may contain some structural defects and charge traps. Moreover, when the ZnO seeds were sputtered on the AAO layer, some entered into the nanopores of the AAO layer, which led to reduction of the effective thickness of the insulating layer. Consequently, the current leakages might have occurred through the AAO layer due to hopping conduction mechanism between the ZnO NWs and the bottom Al electrode. Thereby reducing the leakage

effect with the increased thickness of the AAO layer, the output performance was enhanced.

In this study, the insulating AAO layer fabricated by the anodization process was not pure  $\text{Al}_2\text{O}_3$ . During the anodization process in sulfuric acid,  $\text{Al}^{3+}$  ions migrate from the Al across the Al/ $\text{Al}_2\text{O}_3$  interface into the formed  $\text{Al}_2\text{O}_3$  layer. While over half of the  $\text{Al}^{3+}$  ions contribute to the formation of the  $\text{Al}_2\text{O}_3$  layer, the remaining  $\text{Al}^{3+}$  ions do not participate in the reaction with oxygen ions and eventually are dissolved into the acid solution.<sup>[19]</sup> At the end of the anodization process, the aluminum oxide layer contains impurities, including  $\text{Al}^{3+}$  ions.<sup>[20]</sup> As a result, they can screen the piezoelectric potential generated by the ZnO nanowires. Since the quantity of the ions in the AAO layer increases with the volume of the AAO layer (at constant ion density), this screening effect is proportional to the thickness of the AAO layer. In order to investigate the effect of these impurities in the AAO layer, the resistances of the AAO layer and electron-beam-evaporated aluminum oxide were calculated by measuring current leakages. The resistance of the AAO layer was a few thousand times lower than that of the evaporated aluminum oxide of equivalent thickness, and also the resistance of the AAO layer with a thickness of 300 nm was larger than that with a thickness of 100 nm (Supporting Information, Figure S8). It means that the current leakage decreases as the thickness of the AAO increases. To understand the screening effect of the impurities, FEM simulation was performed as a function of the  $\text{Al}_2\text{O}_3$  thickness from 100 nm to 2000 nm with various fixed charge densities, including  $1 \times 10^{17}$ ,  $5 \times 10^{17}$ ,  $1 \times 10^{18}$ ,  $5 \times 10^{18}$ , and  $1 \times 10^{19}$   $\text{m}^{-3}$ . The simulation result shows that the  $\Delta V$  gradually decreased with the increase of the  $\text{Al}_2\text{O}_3$  thickness due to the increased quantity of the fixed charges in the AAO, (Supporting Information, Figure S9). Furthermore, the  $\Delta V$  became smaller as the fixed charge density increased, and the decreasing trend of the  $\Delta V$  with the increase of the AAO thickness remained the same regardless of the fixed charge density. In other words, because the influence from the current leakage is larger than that from the screening effect when the thickness of the AAO layer was thinner than 920 nm, the output performance increased with the thickness of the AAO layer, which is different from the simulation result. Once the thickness of the AAO layer is larger than 920 nm, the leakage effect is largely suppressed, so that the experimental result agrees to the simulated result.

Finally, the performance of the NG with a 620-nm-thick AAO layer was measured by varying the bending direction under the same condition, with considering the polarity of the ZnO NWs. Since the ZnO NWs were vertically grown onto the sputtered ZnO seed layer above the AAO layer, the top of the ZnO NWs has a positive potential when the NW layer is compressively strained or a negative potential when the NW layer is tensile strained. Therefore, if the decrease of the output voltage was caused by the screening effect from the current leakages and from the impurities according to our assumption, the screening effect should vary with the bending direction. The output voltage and the current were about three times higher when the NW layer was compressively strained than when it was tensile strained, as shown in Figure 3a,b. This result may be understood by considering two factors. The first factor is that, due to the large difference between the thicknesses of

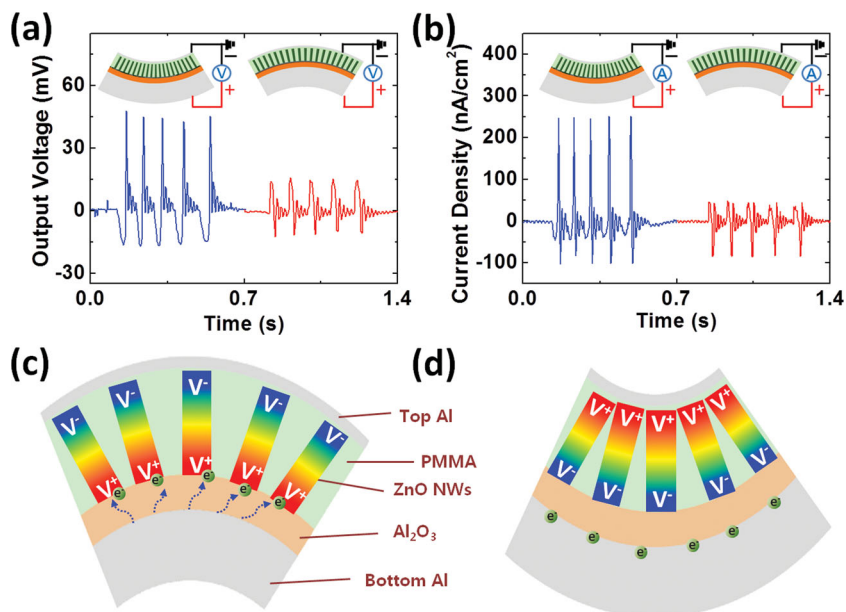


**Figure 3.** Output performance of the NG device depending on the bending direction. a) Output voltage and b) output current when the NG is compressively (inward bending) or tensile (outward bending) strain. Output voltage and the current are about three times higher when the NW layer was compressively strained than when it was tensile strained, possibly due to the screening effect coming from the AAO to the positive piezopotential end. Analysis of the screening effect under c) tensile strain and d) compressive strain condition.

the bottom Al foil and the top Al thin film as shown in Figure 1b, the ZnO NW layer is located at the upper part of the entire NG, so that the strain created in ZnO NW layer may be different between the compressive straining case (inward bending) and that in the tensile straining case (outward bending). However, the strain across the ZnO NW layer showed the same amplitude regardless of the bending direction because the distance from the neutral axis to the ZnO NW layer does not change (Supporting Information, Figure S10). Therefore, the most dominant effect may be related to the screening effect near the bottom of the ZnO NWs. The bottom of the NWs has positive potential when the NW layer is tensile strained, which can be screened by the electrons coming from the current leakage through the AAO layer, as shown in Figure 3c. On the other hand, since the bottom of the NWs has a negative potential when it is compressively strained, the screening effect is significantly decreased, as shown in Figure 3d. This expected result agrees with our observation.

The high sensitivity of the super-flexible NG enables us to measure even a slight local deformation on one's eyelid caused by the motion of the eye ball underneath. The motion of the eye ball is associated with one's sleep pattern that consists of two types:

non-rapid eye movement (NREM) sleep also known as quiet sleep and rapid eye movement (REM) sleep also known as active sleep.<sup>[21–23]</sup> Furthermore, since there are rich sensory and motor connections between the eye and the brain, the motion of the eye ball can provide valuable signs, associated with tiredness as well as brain activity.<sup>[24]</sup> To demonstrate the high sensitivity of the NG for detecting the local deformation on the eyelid according to the motion of the eye ball, the NG with the active area of 3 mm × 10 mm was prepared. The device was attached to a right eyelid, putting the top Al electrode face down on the eyelid in order to get the NW layer strained in compression during the eye ball motion for higher sensitivity, as shown in Figure 4a. The device was firmly attached on the eyelid with eyelash glue. The NG was driven by moving the eye ball from side to side, and the output voltage and current were measured under slow and rapid eye movement, respectively. While moving the eye ball from side to side, the NG is strained as the eye ball passes near the center of the NG, and then the NG is released as the eye arrives at the other side. As a result, when

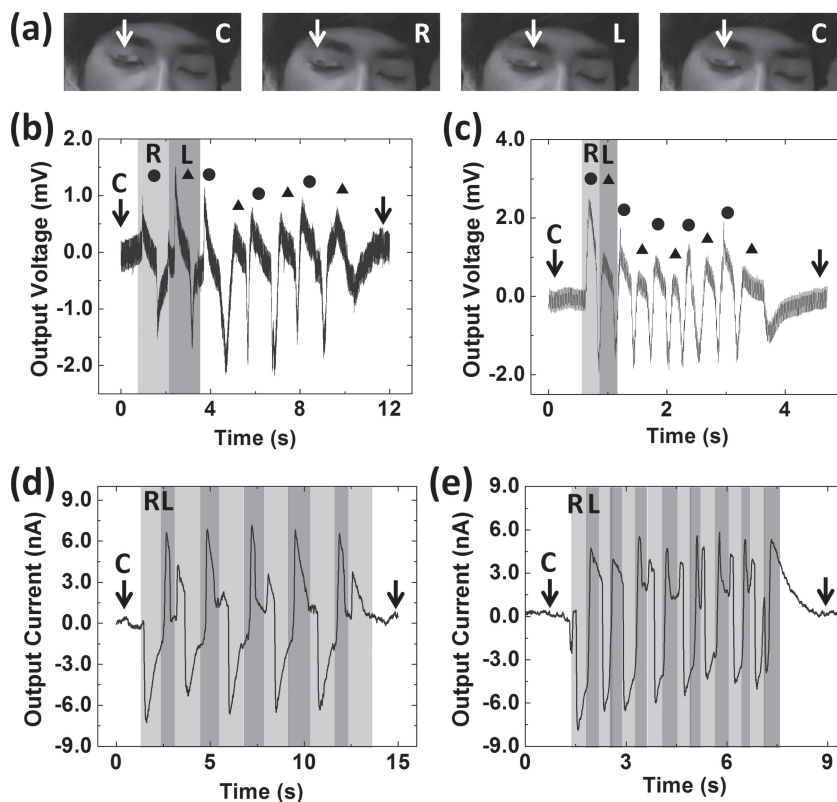


**Figure 4.** Super-flexible NG as an active sensor for detecting the motion of a human eye ball. a) The NG attached a right eyelid was driven by moving the eye ball from right (R), center (C), and to left (L) or from L, C, and R. Output voltage measured under b) slow and c) rapid eye movement. Output current measured under d) slow and e) rapid eye movement.

the eye ball moves from left to right or from right to left, the output indicates one-cycle of an alternating signal caused by the piezoelectric potential; a single peak is detected while moving the eye ball from one end to the center of the NG, and the opposite peak is detected while moving the eye ball from the center to the other end of the NG. Figure 4b shows the output voltage of the NG measured under the slow motion of the eye ball ( $\approx 0.4$  Hz). The output voltage was observed as four-cycle alternating signals during four round-trips of the right eye (Figure 4b and Supporting Information, Video 1). Furthermore, under the rapid eye movement ( $\approx 1.6$  Hz) of five round-trips, the measured output voltage clearly showed five-cycle alternating signals following the motion of eye ball (Figure 4c and Supporting Information, Video 1). The output current was then investigated according to the rapid and the slow eye movement, as shown in Figure 4d,e, and Supporting Information, Video 2. However, each of one-cycle alternating signals in the output current could not be separately obtained under both the rapid and the slow eye movement; whenever moving the eye ball from side to side, portion of them showed one-cycle alternating signal while others showed either a positive or a negative peak. In other words, the signal generated by the motion of the eye ball in one direction was over covered by that from the following motion of the eye ball in the opposite direction due to the time-constant response of the output current. Thus, the output voltage can be effectively utilized to detect the eye ball motion for monitoring sleep pattern, tiredness, and possible brain activity.

The eye tracking system based on our device can be effective in various ways, because almost all of our physical activities rely on our vision. For instance, it can provide a communication system for disabled, allow human computer interaction (HCI), as well as aid cognitive studies and fatigue detection.<sup>[25–27]</sup> Furthermore, our device can track eye movement when no visual activity is taken part such as when measuring the sleep cycle and sleep pattern.<sup>[21]</sup> This is impossible for a system that tracks corneal reflections of infrared light.<sup>[28]</sup> Other major methods are using contact lens with magnetic field sensor on eyes or using electrooculograms (EOG) that detects cornea-retinal potential.<sup>[21,29]</sup> However, both the above mentioned methods require not only a power supply but also a second device to collect information that makes it difficult to track eye movement during ordinary activities such as walking or driving. Our device, however, is self-powered, extremely light and durable. We can reduce the size drastically to allow smooth motion of the skin and yet the signal will be powerful enough even after unforeseen deformation.

### 3. Conclusions

In summary, we have developed a strategy for fabricating ultrathin NG, which has been demonstrated as an active sensor for monitoring tiny skin deformation. The AAO grown on the Al foil by the anodizing process was used not only as an insulating layer between the ZnO NWs and the bottom Al electrode, but also as enhancing mechanical durability between the AAO and the ZnO seed layer due to the covalent bond by sharing oxygen atoms and the increased surface area by the nanopores

of the AAO. The high-sensitive super-flexible NG device was developed by theoretically and experimentally investigating the output performance of the NG by varying the thickness of the AAO layer. Furthermore, the high-sensitive NG demonstrated the potential to work as an active deformation sensor capable of detecting a slight eyelid behavior under the motion of the eye ball for monitoring sleep pattern, tiredness and possible brain activity. Our strategy can provide a highly promising platform as a self-powered sensor for smart skin applications.

### 4. Experimental Section

**Synthesis of ZnO NWs:** ZnO NWs were grown on the seed layer by a hydrothermal process at 95 °C for 5 h in mechanical convection oven (model Yamato DKN300, Santa Clara, CA). The nutrient solution for the growth of ZnO NWs was an aqueous solution of 0.05 M hexamethylenetetramine (HMTA) and 0.05 M zinc nitrate hexahydrate ( $\text{ZnNO}_3 \cdot 6(\text{H}_2\text{O})$ ). During the growth, the substrates were placed at the top of the solution with one face down. The ZnO NWs-grown substrates were rinsed with DI water and gently blown with nitrogen gas.

**Preparation of AAO Layer with Different Thickness:** Al foils were anodized at a constant voltage of 25 V in 0.3 M sulfuric acid solution at  $\approx 0$  °C. In the anodization process, AAO layers with different thicknesses were prepared by controlling the anodizing time. The anodizing times of 10, 12, 14, 16, 18 min lead to the AAO layer thicknesses of 280, 620, 920, 1220, and 1440 nm, respectively.

### Supporting Information

Supporting Information is available from the Wiley Online Library or from the author.

### Acknowledgements

Research was supported by Airforce, U.S. Department of Energy, Office of Basic Energy Sciences (Award DE-FG02-07ER46394), NSF (0946418), MANA, National Institute For Materials, Japan, a joint project with Sungkyunkwan University, Korea, and the Knowledge Innovation Program of the Chinese Academy of Science (Grant No. KJCX2-YW-M13). The Region Rhone-Alpes contributed to financial support the exchange program of one of the authors (RH). Part of the research leading to these results has received funding from the European Community's Seventh Framework Programme (FP7/2007–2013) under grant agreement NANOFUNCTION No.257375.

Received: June 8, 2013

Revised: August 8, 2013

Published online:

- [1] Z. L. Wang, W. Wu, *Angew. Chem.* **2012**, *51*, 11700.
- [2] N. S. Lewis, *Science* **2007**, *315*, 798.
- [3] D. Kramer, B. Poudel, H.-P. Feng, J. C. Caylor, B. Yu, X. Yan, Y. Ma, X. Wang, D. Wang, A. Muto, K. McEnaney, M. Chiesa, Z. Ren, G. Chen, *Nat. Mater.* **2011**, *10*, 532.
- [4] P. D. Mitcheson, E. M. Yeatman, G. K. Rao, A. S. Holmes, T. C. Green, *Proc. IEEE* **2008**, *96*, 1457.
- [5] Z. L. Wang, J. H. Song, *Science* **2006**, *312*, 242.
- [6] S. Xu, Y. Qin, C. Xu, Y. Wei, R. Yang, Z. L. Wang, *Nat. Nanotechnol.* **2010**, *5*, 366.

- [7] Y. Hu, Y. Zhang, C. Xu, L. Lin, R. L. Snyder, Z. L. Wang, *Nano Lett.* **2011**, *11*, 2572.
- [8] C. Chang, V. H. Tran, J. Wang, Y.-K. Fuh, L. Lin, *Nano Lett.* **2010**, *10*, 726.
- [9] C. Sun, J. Shi, D. J. Bayerl, X. Wang, *Energy Environ. Sci.* **2011**, *4*, 4508.
- [10] S. Lee, J.-I. Hong, C. Xu, M. Lee, D. Kim, L. Lin, W. Hwang, Z. L. Wang, *Adv. Mater.* **2012**, *24*, 4398.
- [11] Z. Li, Z. L. Wang, *Adv. Mater.* **2010**, *23*, 84.
- [12] Y. Hu, C. Xu, Y. Zhang, L. Lin, R. L. Snyder, Z. L. Wang, *Adv. Mater.* **2011**, *23*, 4068.
- [13] A. Yu, P. Jiang, Z. L. Wang, *Nano Energy* **2012**, *1*, 418.
- [14] R. Zhang, L. Lin, Q. Jing, W. Wu, Y. Zhang, Z. Jiao, L. Yan, R. P. S. Han, Z. L. Wang, *Energy Environ. Sci.* **2012**, *5*, 8528.
- [15] L. Lin, Y. Hu, C. Xu, Y. Zhang, R. Zhang, X. Wen, Z. L. Wang, *Nano Energy* **2013**, *2*, 75.
- [16] S. Lee, S.-H. Bae, L. Lin, Y. Yang, C. Park, S.-W. Kim, S. N. Cha, H. Kim, Y. J. Park, Z. L. Wang, *Adv. Funct. Mater.* **2013**, *23*, 2445.
- [17] Z. L. Wang, G. Zhu, Y. Yang, S. Wang, C. Pan, *Materials Today* **2012**, *15*, 532.
- [18] H.-M. Xiong, Z.-D. Wang, D.-P. Liu, J.-S. Chen, Y.-G. Wang, Y.-Y. Xia, *Adv. Funct. Mater.* **2005**, *15*, 1751.
- [19] G. E. J. Poinern, N. Ali, D. Fawcett, Progress in nano-engineered anodic aluminum oxide membrane development. *Materials* **2011**, *4*, 487.
- [20] G. E. Thomson, G. C. Wood, Anodic films on aluminum, in *Treatise on Materials Science and Technology* (Ed: J. C. Scully), Academic Press, New York **1983**, *23*, Ch. 5, pp. 205–329.
- [21] E. Aserinsky, N. Kleitman, *Science* **1953**, *118*, 273.
- [22] P. Maquet, J. M. Péters, J. Aerts, G. Delfiore, C. Degueudre, A. Luxen, G. Franck, *Nature* **1996**, *383*, 163.
- [23] M. A. Carskadon, W. C. Dement, *Princ. Pract. Sleep Med.* **1994**, *4*, 13.
- [24] S. K. L. Lal, A. Craig, *Biol. Psychol.* **2011**, *55*, 173.
- [25] J. R. LaCourse, F. C. Hludik Jr., *Bio IEEE Trans. Biomed. Eng.* **1990**, *37*, 1215.
- [26] A. Poole, L. J. Ball, Eye tracking in HCI and usability research. *Encyclopedia of Human-Computer Interaction* (Ed: C. Ghaoui), Idea Group, PA **2006**, pp. 211–219.
- [27] K. Rayner, *Psychol. Bull.* **1998**, *124*, 372.
- [28] D. W. Hansen, Q. Ji, *IEEE Trans. Pattern Anal. Mach. Intell.* **2010**, *32*, 478.
- [29] D. A. Robinson, *IEEE Trans. Biomed. Electron.* **1963**, *10*, 137.